Electronic Supplementary Information (ESI)

Controlling exciton lifetime of blue thermally activated delayed fluorescence emitters using heteroatom contained pyridoindole donor moiety

Gyeong Heon Kim, Raju Lampande, Joon Beom Im, Jung Min Lee, Ju Young Lee*, and Jang Hyuk Kwon*

Department of Information Display, Kyung Hee University, 26, Kyungheedae-ro, Dongdaemoon-gu, Seoul, 02447, Republic of Korea.
E-mail: juyoung105@khu.ac.kr, jhkwon@khu.ac.kr

Contents

1. Experimental section

1.1. General Information

To synthesize TADF emitters, all reagents and solvents were purchased from Aldrich Chemical Co. and TCI. To verify molecular structures of synthesized TADF emitters, ^{1}H- and ^{13}C-NMR spectrum was measured using Bruker Avance 400 NMR spectrometer. Low and high-resolution mass spectra were performed using JEOL JMS-600W Gas Chromatography-Mass spectrometer. UV-vis absorption and photoluminescence (PL) spectra were measured using SCINCO S-4100 spectrometer and JASCO FP-8500 spectrometer, respectively. The photoluminescence quantum yields (PLQYs) measurements were performed using integrated sphere. The transient PL decay of thin film was recorded using a Quantaurus-Tau fluorescence lifetime measurement system (C11367-03, Hamamatsu Photonics Co.) in N_2 filled atmosphere. Cyclic voltammetry (CV) was executed using EC epsilon electrochemical analysis equipment.

1.2. Material synthesis

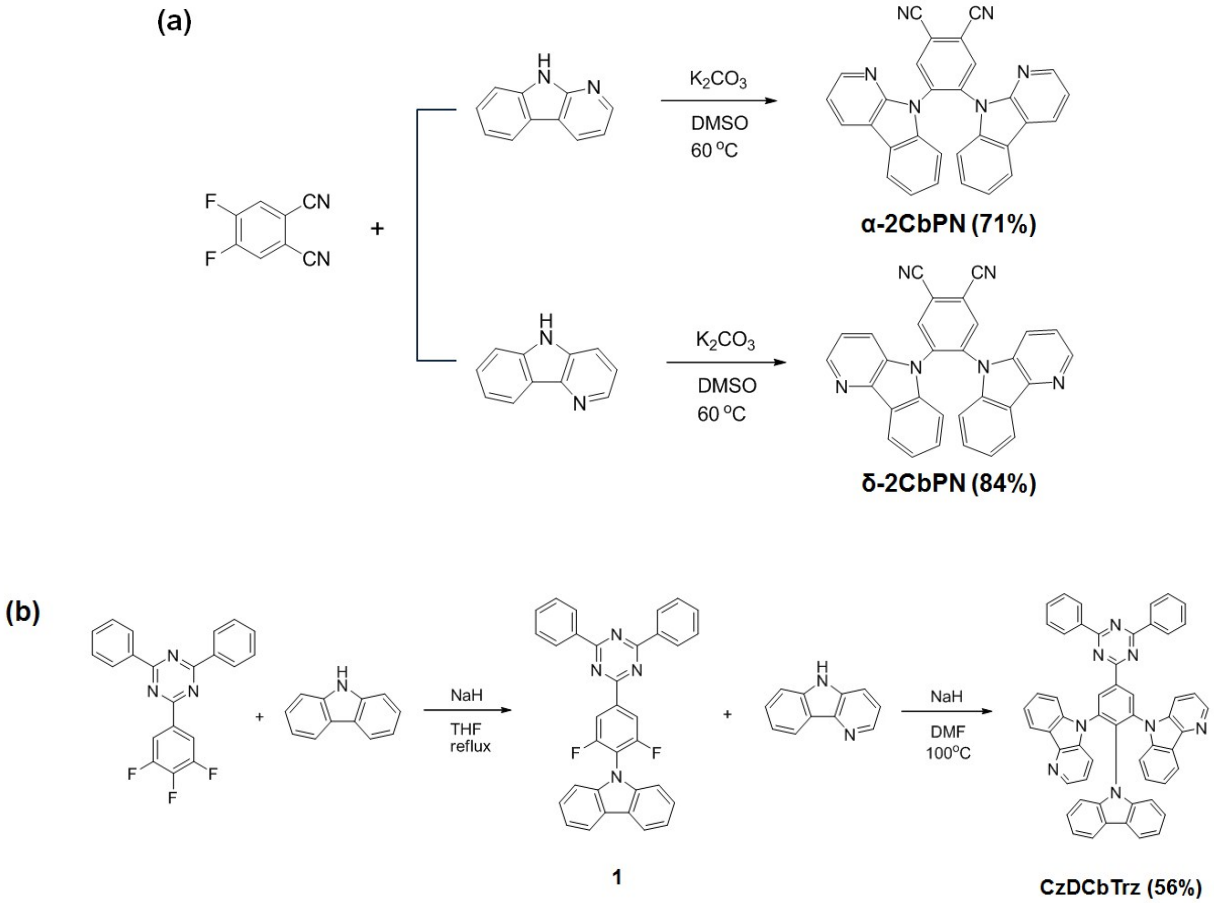

Scheme 1 Synthetic routes of (a) **α-2CbPN, δ- 2CbPN** and (b) **CzDCbTrz**.

Synthesis of 4,5-bis(9H-pyrido[2,3-b]indol-9-yl)phthalonitrile (α-2CbPN)

9H-Pyrido[2,3-b]indole (6.2 g, 36.6 mmol) was added to a mixture of K_2CO_3 (7.6 g, 54.9 mmol) in DMSO (60 mL). After the mixture was stirred at room temperature for 1 h, 4,5-difluorophthalonitrile (2.0 g, 12.2 mmol) was added, and then the mixture was stirred at room temperature for 2 h and at 50°C for an additional 15 h. After cooling, the mixture was poured into water, and the precipitate was filtered and dried. The crude product was dissolved in CH_2Cl_2 and the resulting solution was filtered through silica gel and concentrated. The crude product was recrystallized from methanol and CH_2Cl_2 to produce a pale brown solid (4.0 g, a 2.1:1 mixture of stereoisomers, 71%). Major compound: ^{1}H-NMR ($CDCl_3$, 400 MHz): δ [ppm] 8.38 (s, 2H), 8.34 (dd, J = 4.8, 1.2 Hz, 2H), 8.23 (d, J = 7.6 Hz, 2H), 7.51 (m, 2H), 7.43 (m, 2H), 7.40 (m, 2H), 7.02 (d, J = 8.4 Hz, 2H), 6.77 (dd, J = 8.4, 4.8 Hz, 2H). ^{13}C-NMR ($CDCl_3$, 125 MHz): δ [ppm] 144.2, 142.8, 139.1, 137.4, 135.3, 131.5, 128.9, 123.6, 123.1, 121.6, 120.0, 116.1, 115.6, 114.1, 108.7. HRMS-FAB (m/z): [M+H]+ calculated for $C_{30}H_{16}N_6$, 461.1515; found, 461.1515.

Synthesis of 4,5-bis(5H-pyrido[3,2-b]indol-5-yl)phthalonitrile (δ-2CbPN)

A procedure similar to that used for **α-2CbPN** was followed but with 5H-pyrido[3,2-b]indole (6.2 g, 36.6 mmol) instead of 9H-pyrido[2,3-b]indole. The crude product was recrystallized from methanol and CH_2Cl_2 to produce a pale yellow solid (4.7 g, a 1.3:1 mixture of stereoisomers, 84%). Major compound: ^{1}H-NMR ($CDCl_3$, 400 MHz): δ [ppm] 8.47 (s, 2H), 8.33 (dd, J = 4.8, 1.2 Hz, 2H), 8.13 (dd, J = 7.6, 1.6 Hz, 2H), 7.69 (d, J = 7.6 Hz, 2H), 7.23 (dd, J = 7.6, 4.8 Hz, 2H), 7.14 (s, 2H), 7.02 (m, 2H), 6.88 (d, J = 8.0 Hz, 2H). ^{13}C-NMR ($CDCl_3$, 125 MHz): δ [ppm] 150.3, 146.0, 137.1, 136.4, 136.4, 128.5, 126.5, 122.0, 121.8, 120.6, 117.6, 117.1, 114.9, 114.8, 110.2. HRMS-FAB (m/z): [M+H]+ calculated for $C_{30}H_{16}N_6$, 461.1515; found, 461.1517.

Synthesis of 9-(4-(4,6-diphenyl-1,3,5-triazin-2-yl)-2,6-difluorophenyl)-9H-carbazole (1)

9H-Carbazole (1.0 g, 6.1 mmol) in tetrahydrofuran (60 ml) was added to sodium hydride (60%, 484 mg, 12.1 mmol). After stirring for 30 min, 2,4-diphenyl-6-(3,4,5-trifluorophenyl)-1,3,5-triazine (2.2 g, 6.1 mmol) was added into the solution. The resulting solution was refluxed for 5 h under nitrogen and cooled down to room temperature. The reaction mixture was concentrated and diluted with ethyl acetate. The resulting suspension was filtered and washed with ethyl acetate and distilled water. The crude product was recrystallized from toluene to afford the title compound (2.4 g, 78%) as a white solid. ^{1}H-NMR (400 MHz, $CDCl_3$): δ [ppm] 8.83 (m, 4H), 8.64 (d, J=8.4 Hz, 2H), 8.19 (d, J=7.6 Hz, 2H), 7.62-7.71 (m, 6H), 7.51 (t, J=8.0 Hz, 2H), 7.38 (t, J=7.2 Hz, 2H), 7.28 (s, 1H), 7.26 (d, J= Hz, 1H).

Synthesis of 5,5'-(2-(9H-carbazol-9-yl)-5-(4,6-diphenyl-1,3,5-triazin-2-yl)-1,3-phenylene)bis(5H-pyrido[3,2-b]indole) (CzDCbTrz)

5H-Pyrido[3,2-b]indole (2.4 g, 14.1 mmol) in N,N-dimethylformamide (90 ml) was added to sodium hydride (60%, 677 mg, 16.9 mmol). After stirring for 30 min, **1** (2.4 g, 4.7 mmol) was added into the solution. The reaction mixture was stirred at 100 °C for 18 h under nitrogen and cooled down to room temperature. The reaction mixture was concentrated and diluted using 10% methanol/dichloromethane, and then filtered. Finally, the crude product was purified by silica gel chromatography and recrystallized from methanol/dichloromethane to afford the title compound (2.1 g, a 1:1 mixture of stereoisomers, 56%) as a greenish yellow solid. ^{1}H-NMR (400 MHz, CDCl3): δ [ppm] 9.39 (s, 2H), 9.36 (s, 2H), 8.76-8.79 (m, 8H), 8.42 (d, J=4.0 Hz, 2H), 8.36 (m, 2H), 8.24-8.29 (m, 4H), 7.79 (d, J=8.4 Hz, 2H), 7.56-7.67 (m, 16H), 7.37-7.45 (m, 8H), 7.23 (m, 6H), 7.02 (dd, J=8.4, 4.8 Hz, 2H), 6.83-6.90 (m, 8H), 6.64-6.74 (m, 6H); ^{13}C-NMR ($CDCl_3$, 100 MHz): δ [ppm] 172.4, 169.4, 141.4, 141.1, 140.7, 138.6(1), 138.6(0), 137.6(4), 137.6(1), 137.5, 136.7, 136.6, 135.4, 134.7, 134.4, 133.6, 130.0(4), 130.0(0), 129.2, 128.9(5), 128.9(0), 128.3, 125.2, 124.9, 123.8, 123.6, 123.5, 122.0,

121.8, 121.7, 121.3, 121.2, 121.0, 120.9, 120.1, 120.0, 119.9, 119.7, 119.3, 119.2, 117.9, 117.5, 110.0, 109.8, 109.6, 109.4, 109.3. HRMS-FAB (m/z): [M+H]+ calculated for $C_{55}H_{35}N_8$, 807.2985; found, 807.2983.

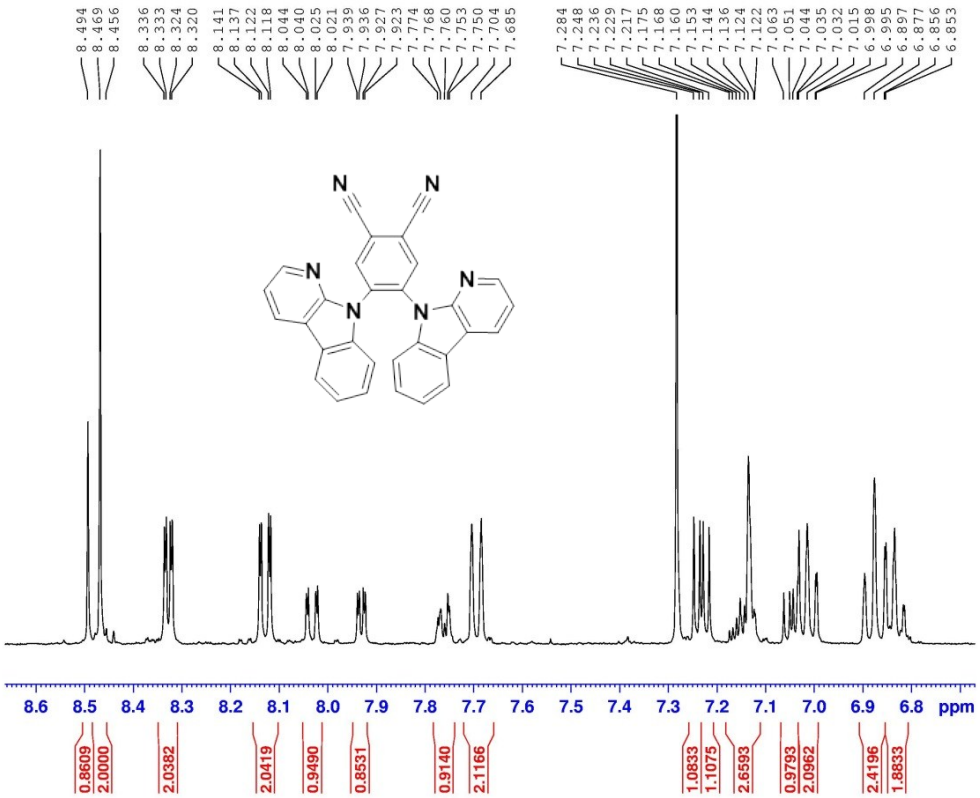

Fig. S1 ^{1}H-NMR spectrum of **α-2CbPN**.

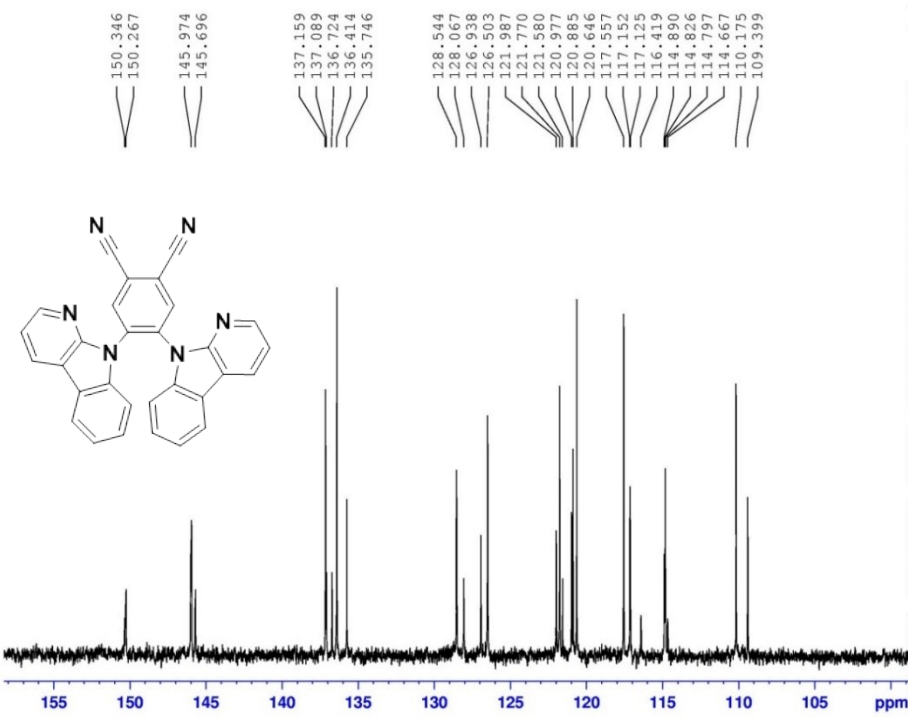

Fig. S2 ^{13}C-NMR spectrum of **α-2CbPN**.

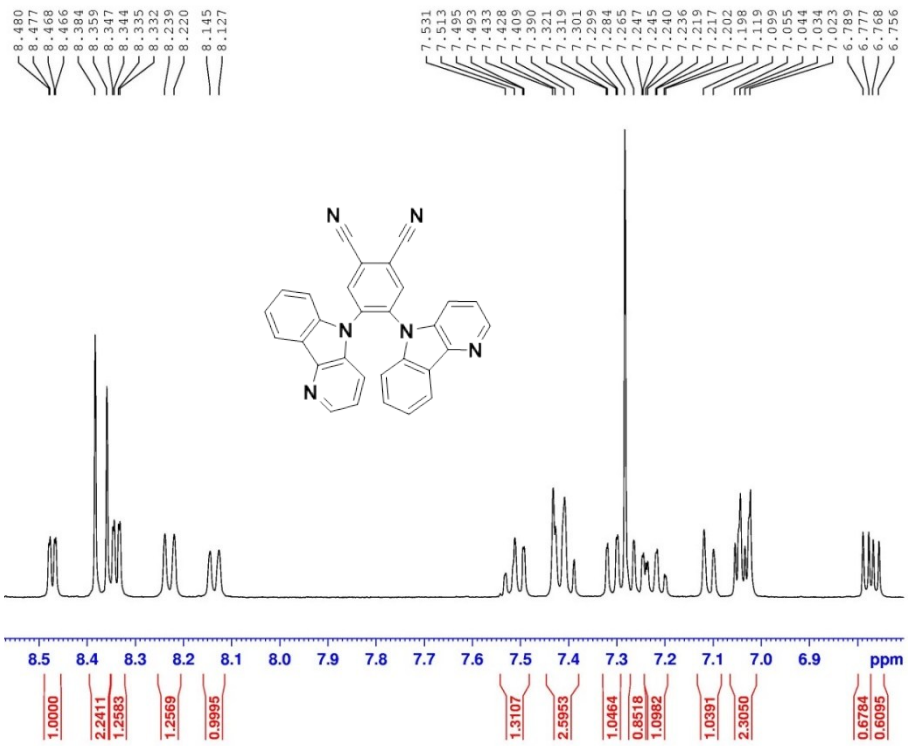

Fig. S3 ^{1}H-NMR spectrum of **δ-2CbPN**.

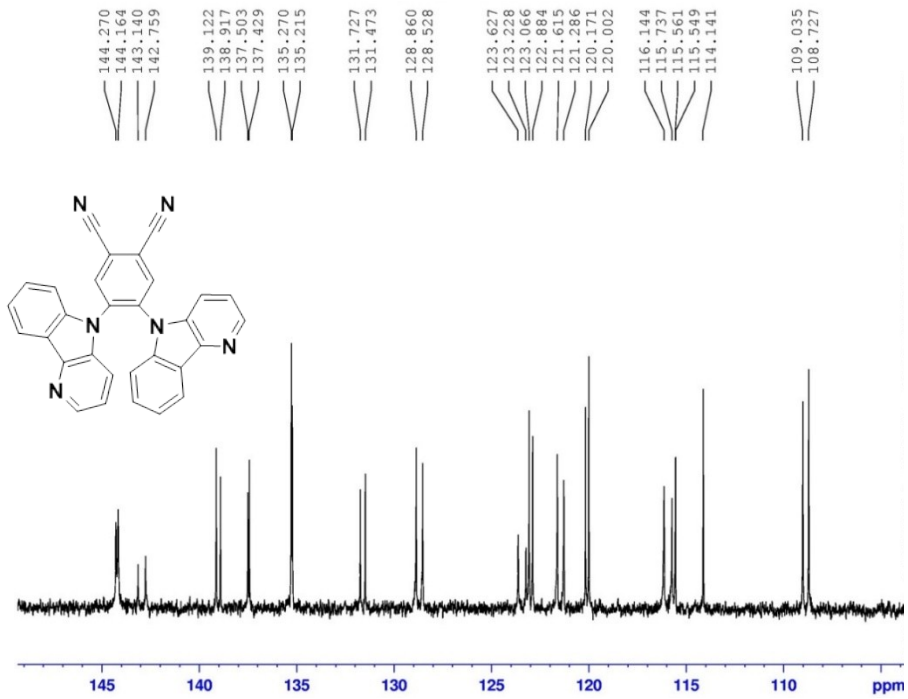

Fig. S4 ^{13}C-NMR spectrum of **δ-2CbPN**.

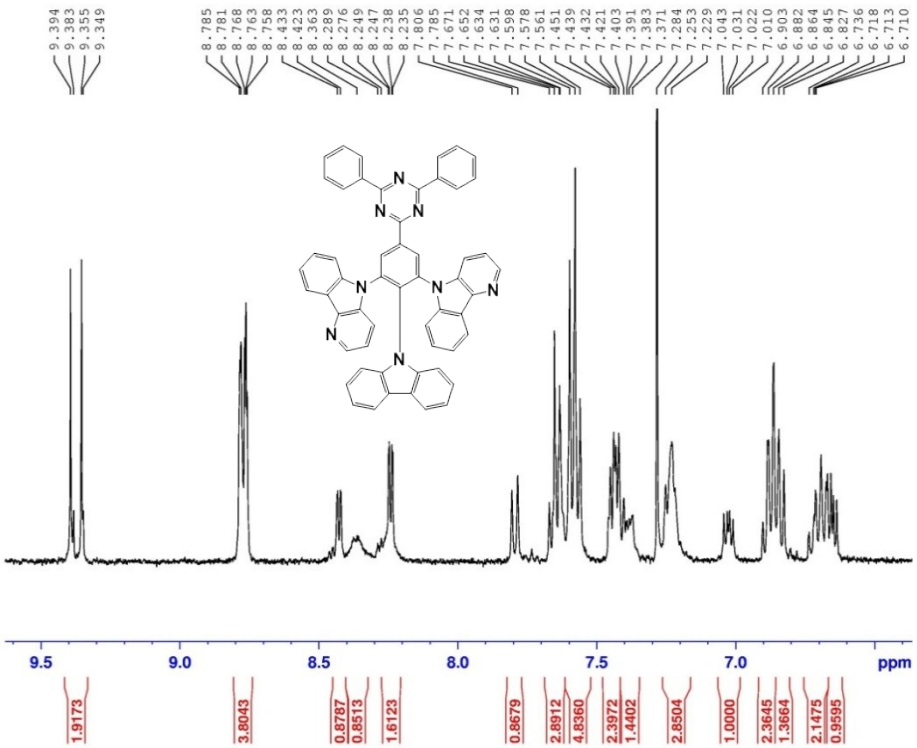

Fig. S5 ^{1}H-NMR spectrum of **CzDCbTrz**.

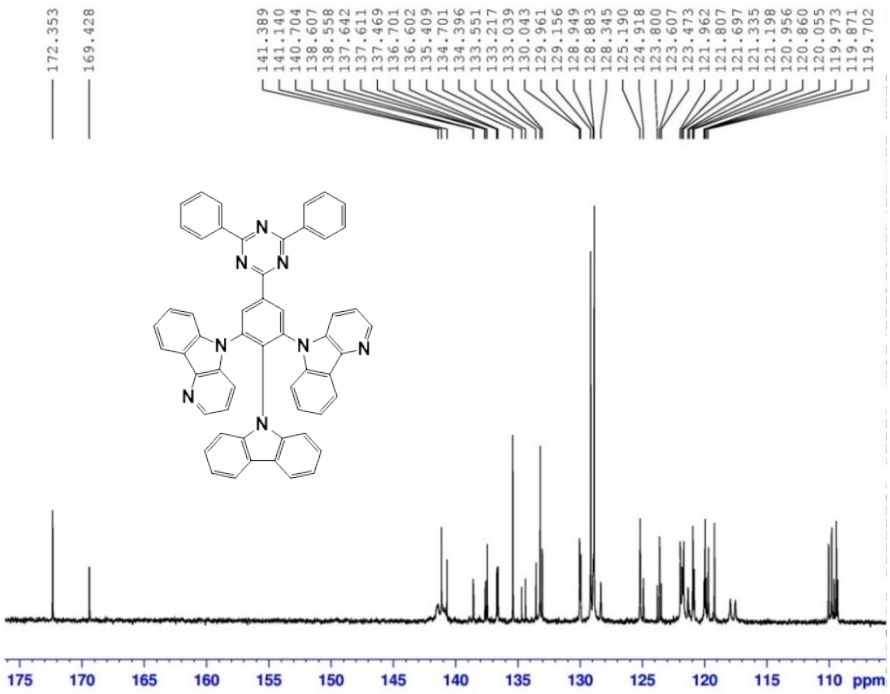

Fig. S6 ^{13}C-NMR spectrum of **CzDCbTrz**.

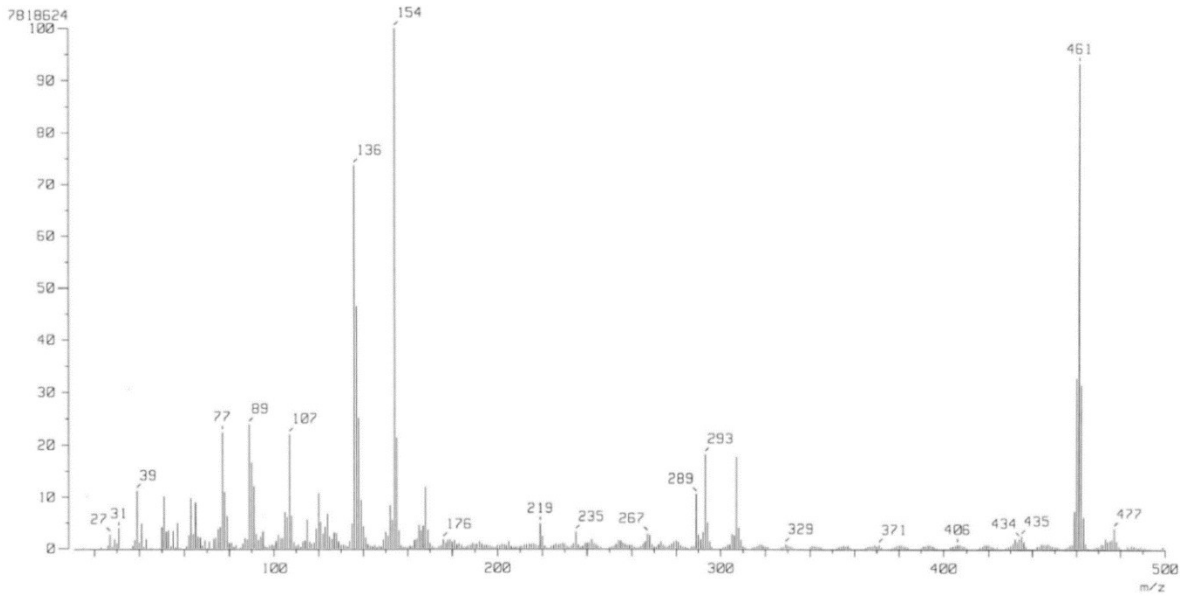

Observed m/z	Int%	Err[ppm / mmu]	U.S.	Composition
461.1515	100.0	+0.0 / +0.0	25.5	C 30 H 17 N 6

Fig. S7 Low and high resolution mass results of **α-2CbPN**.

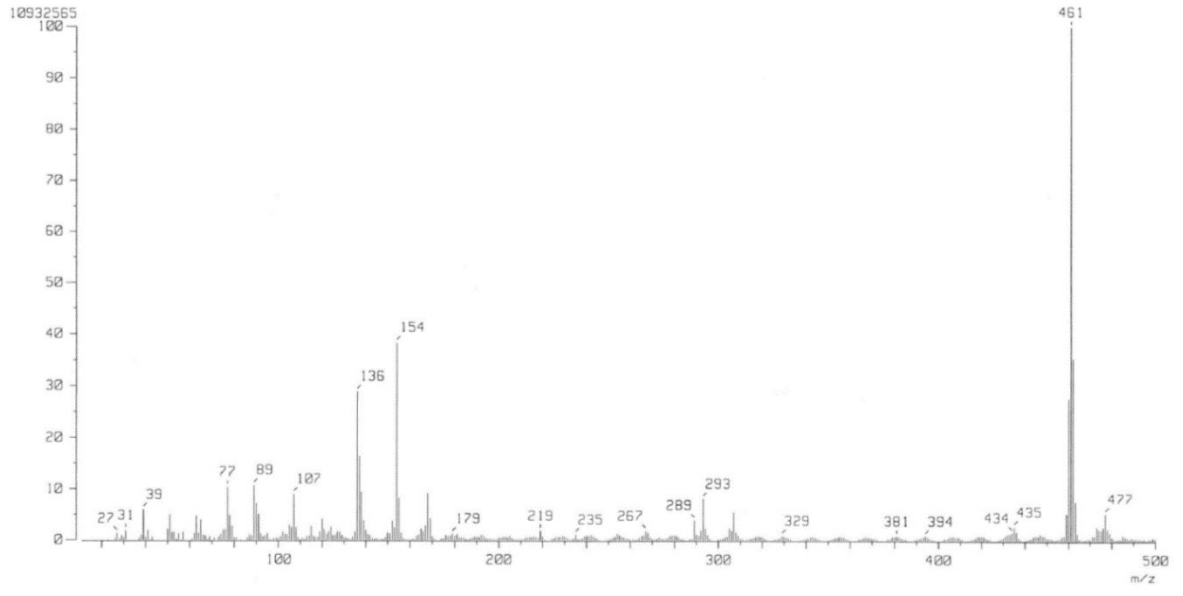

Observed m/z	Int%	Err[ppm / mmu]	U.S.	Composition
461.1517	100.0	+0.6 / +0.3	25.5	C 30 H 17 N 6

Fig. S8 Low and high resolution mass results of **δ-2CbPN**.

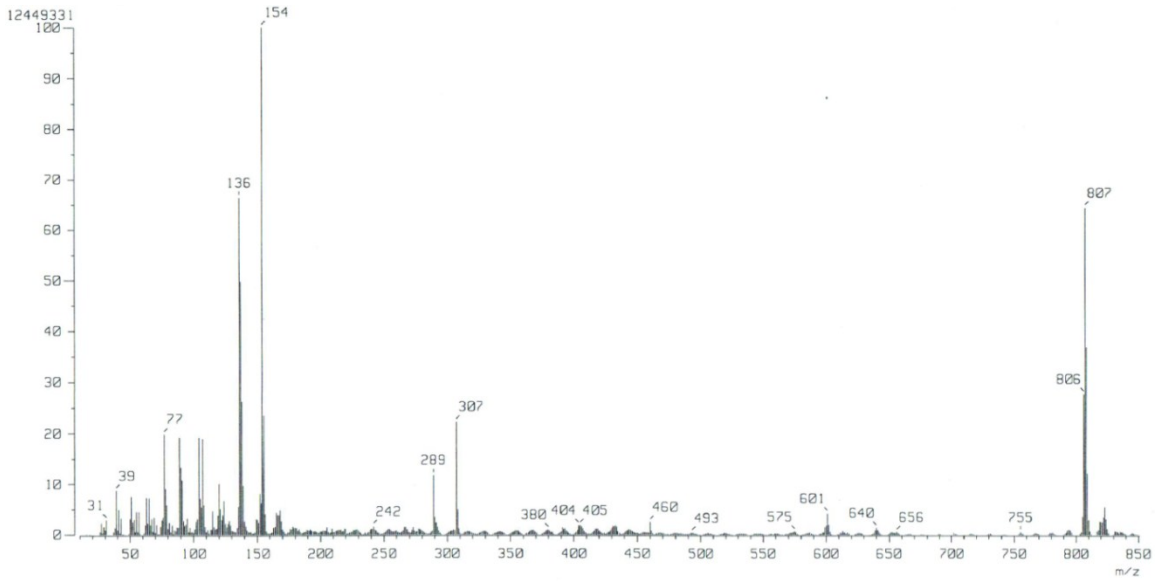

Observed m/z	Int%	Err[ppm / mmu]	U.S.	Composition
807.2983	100.0	-8.5 / -6.9	45.5	C 64 H 39

Fig. S9 Low and high resolution mass results of **CzDCbTrz**.

2. Computational data

To determine the molecular orbitals, energy levels of TADF emitters, density functional theory (DFT/B3LYP) and time dependent density functional theory (TD-DFT/GGA) simulations were executed with the double numerical plus *d*-functions (DND) atomic orbital basis set. The molecular simulations were done using DMol3 module in Material studio 8.0 software package (Accelrys Inc., San Diego, California, United States).

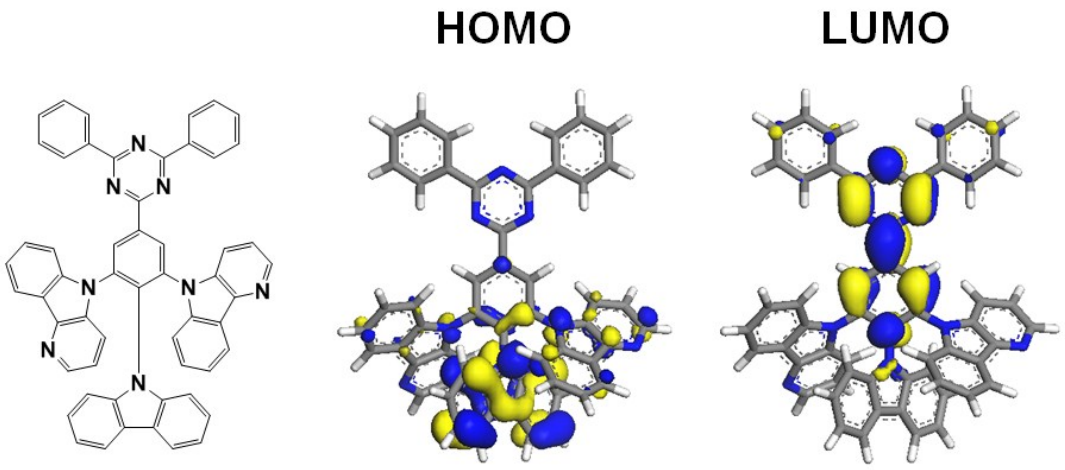

Fig. S10 Chemical structure and distributions of HOMO and LUMO in **CzDCbTrz**.

Table S1 Calculated HOMO, LUMO, band gap, S_1, T_1, ΔE_{ST} values, angles and bond length between donor and acceptor at S_0 and S_1 by B3LYP level.

	HOMO [eV]	LUMO [eV]	T_1 [eV]	ΔE_{ST} [eV]	θ (S_0, S_1) [°]	l (S_0, S_1) [Å]
2CzPN	-5.76	-2.94	2.66	0.16	54.4, 86.5	1.403, 1.446
α-2CbPN	-5.81	-2.76	2.81	0.24	57.7, 87.9	1.406, 1.454
δ-2CbPN	-5.79	-2.91	2.77	0.11	55.9, 85.8	1.404, 1.445
TCzTrz	-5.53	-2.63	2.75	0.15	60.8, 85.4	1.404, 1.444
CzDCbTrz	-5.54	-2.62	2.80	0.12	61.1, 62.3	1.406, 1.421

3. Photo-physical properties

3.1. Solvatochromic effect

The solvent polarity dependent PL characteristics of TADF emitters were evaluated in 10^{-5} M hexane, toluene, methylene chloride (MC), and acetonitrile (ACN) solvents. The PL spectra of synthesized emitters α-2CbPN, δ-2CbPN and CzDCbTrz with respect to different solvent polarity are demonstrated in below Figure S11. Strong solvatochromic effect was observed in all the three TADF emitters due to the different polarity of solvents.

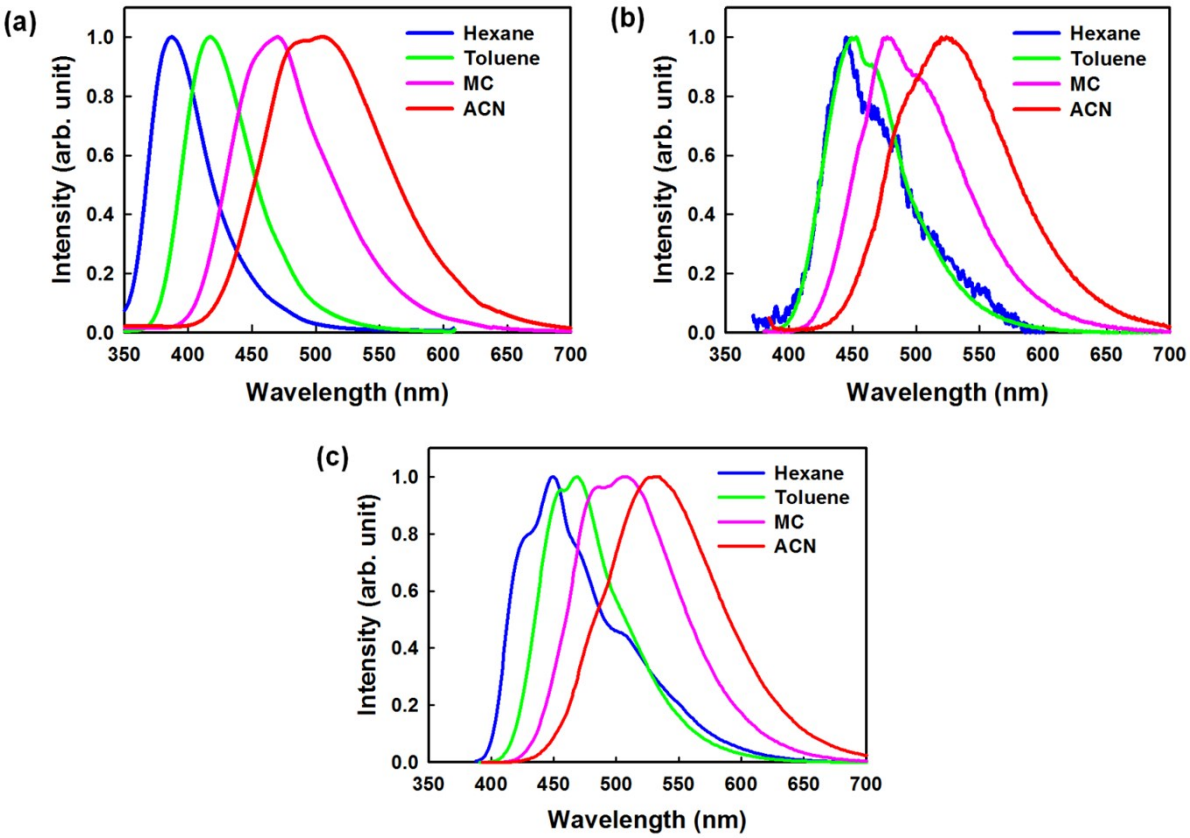

Fig. S11 Solvent dependent PL spectra of (a) **α-2CbPN** (b) **δ-2CbPN** and (c) **CzDCbTrz** at room temperature (300 K).

3.2. UV-Vis absorption, fluorescent and phosphorescent spectra

UV-Vis absorption spectra was measured in 10^{-5} M toluene solution. The prompt and delayed fluorescent spectrum were measured from 0 s to 40 μs and from 40 μs to 1 ms after photo-excitation at room temperature (300 K). The phosphorescent spectra was obtained from 1 ms to 10 ms after photo-excitation at low temperature (77 K). PL spectrum of 2CzPN, α-2CbPN, and δ-2CbPN were measured in 20 wt% doped mCP host film, and TCzTrz, CzDCbTrz emitters were measured in 6 wt% doped DPEPO host film.

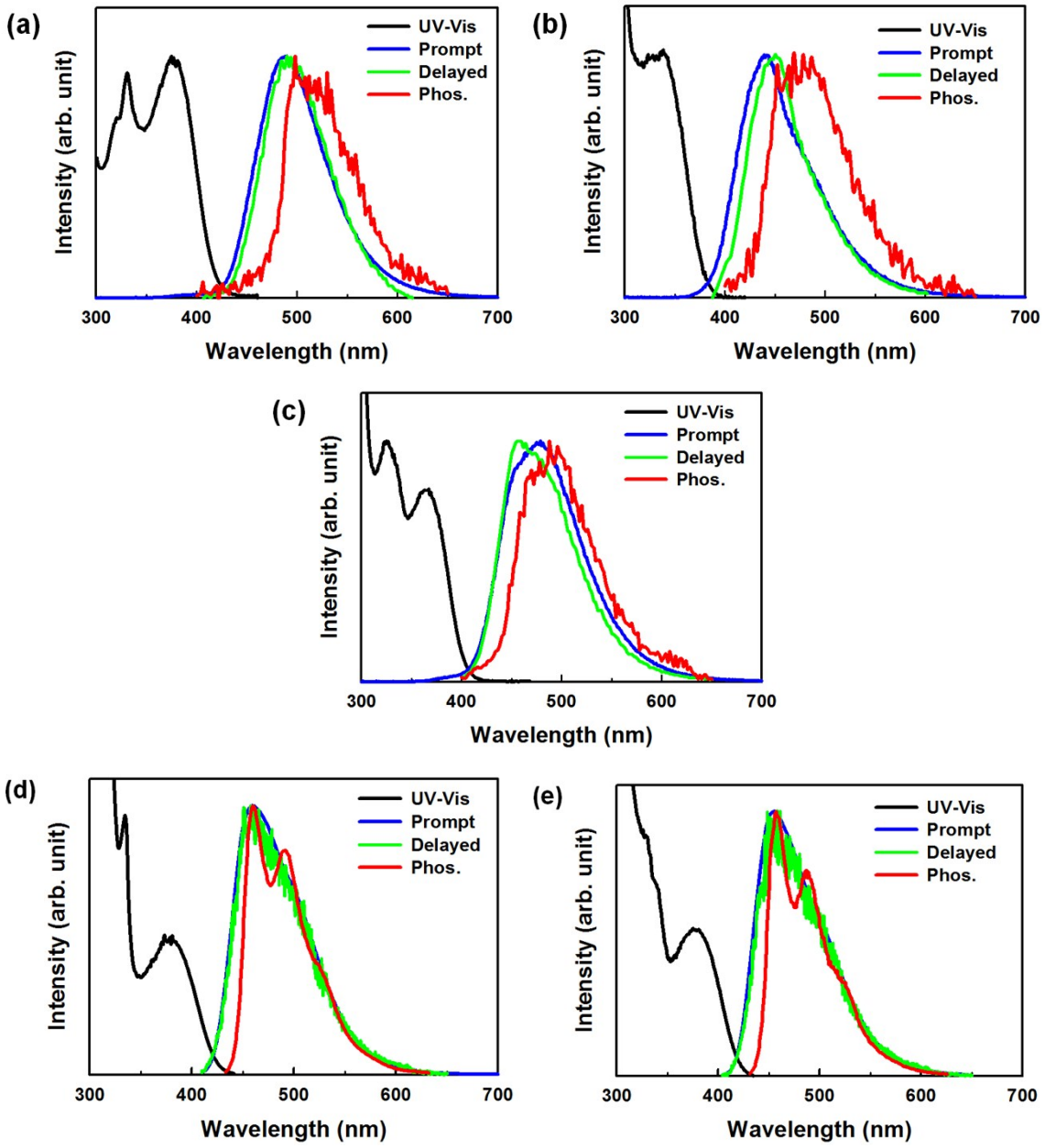

Fig. S12 UV-Vis absorption, normalized prompt and delayed fluorescent spectra at 300 K, and phosphorescent spectra at 77 K of (a) **2CzPN** (b) **α-2CbPN** (c) **δ-2CbPN** (d) **TCzTrz** and (d) **CzDCbTrz**.

4. Electro-chemical properties

Electrochemical analyses of the synthesized TADF emitters were inspected using CV. To measure the CV characteristics of TADF emitters, platinum wire and synthesized material on ITO/glass substrate and Ag wire using 0.1 M $AgNO_3$ in acetonitrile solution were used as counter, working and reference electrodes, respectively. 0.1 M tetrabutyl ammonium perchlorate (Bu_4NClO_4) solution in acetonitrile was used as a supporting electrolyte. Using an internal ferrocene/ferrocenium (Fc/Fc^+) standard, the potential values were converted to the saturated calomel electrode (SCE) scale.

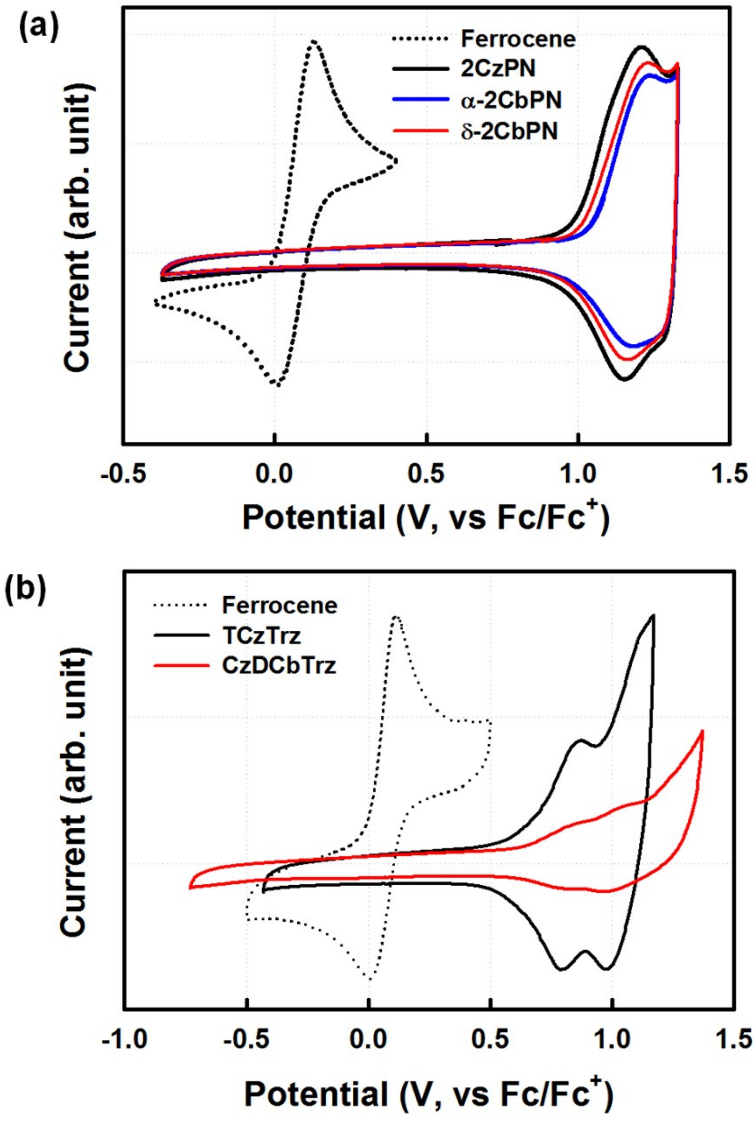

Fig. S13 Cyclic voltammetry analysis of (a) **2-CzPN**, **α-2CbPN** and **δ-2CbPN** and (b) **TCzTrz**, **CzDCbTrz**.

Table S2 UV-Vis absorption, PL and ΔE_g characteristics of TADF emitters.

Emitters	λ_{abs} [a, b] [nm]	λ_{PL} [a] [nm]	ΔE_g [c] [eV]
2CzPN	374	473	2.83
α-2CbPN	338	417	3.13
δ-2CbPN	365	453	2.95
TCzTrz	377	472	2.82
CzDCbTrz	374	469	2.90
[a]Measured in 10^{-5} M toluene solution. [b]Measured from the maximum absorption peak. [c]Measured from the onset of absorption spectra.			

5. Transient PL decay

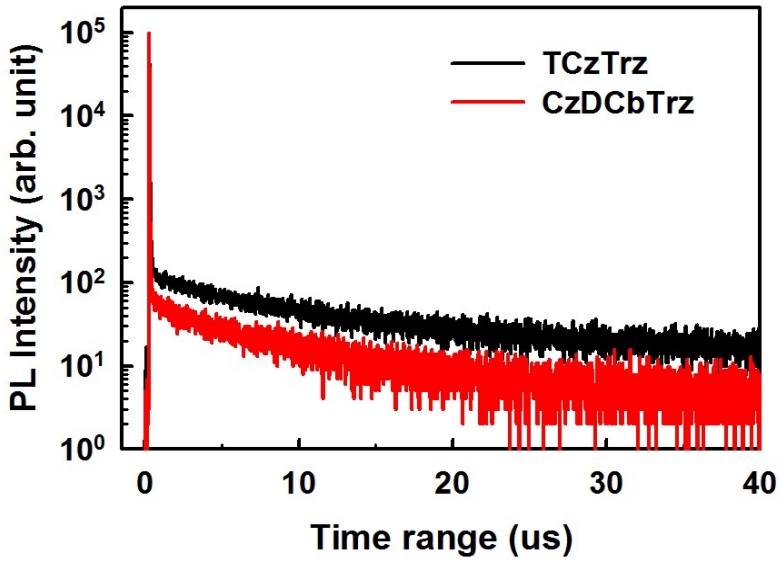

Fig. S14 PL decay curves of **TCzTrz** and **CzDCbTrz** in 6wt% doped DPEPO host at room temperature (300 K) under N_2 filled atmosphere.

6. Equations for the evaluation of rate constants

The rate constants (k_r^S, k_{nr}^S, k_{RISC}, k_{ISC}, k_{nr}^T, k_p and k_d) associated with the important process in TADF emitter are evaluated as follows:

$Herein, k_p$ and k_d denotes prompt and delayed fluorescence rate constants and it can be calculated from the experimently measured prompt and delayed decay time.

$$k_p = \frac{1}{\tau_p} \quad \text{.....(1)}$$

$$k_d = \frac{1}{\tau_d} \quad \text{.....(2)}$$

Furthermore, the prompt and delayed fluorescence quantum efficiency (Φ_F and Φ_{TADF}), can experimentally obtained from PLQY and transient PL and it is also related with the rate constants and their relationship is theoratically given in the previously reported article[1] as follows:

$$\phi_p = \frac{k_r^S}{k_p}\frac{k_r^S + k_{nr}^S + k_{ISC} - k_d}{k_p - k_d} \quad \text{.....(3)}$$

$$\phi_d = \frac{k_r^S}{k_d}\frac{k_p - k_r^S - k_{nr}^S - k_{ISC}}{k_p - k_d} \quad \text{.....(4)}$$

Where, k_r^S is radiative decay rate constant of the singlet state, k_{ISC} is intersystem crossing rate, k_{RISC} is reverse intersystem crossing rate, and k_{nr}^S is non-radiative decay rate constant of the singlet, respectively.

However, to evaluate other rate constants above mentioned equations (1-4) are not sufficient, therefore, certain assumption has to be made to obtain proper equations. Previously, two kinds of assumptions were used in the reported papers[1,2] and these assumptions are i) k_{nr}^S = very small or almost zero, therefore ISC efficiency is 1-Φ_F, ii) non-radiative and radiative decay rate constants of the triplet state $(k_{nr}^T + k_r^T)$ = very small or almost zero and thus Φ_{RISC} =1.

However, it is challenging to calculate both k_{nr}^T and k_{nr}^S at the same time without assuming any one of non-radiative component very small or zero. Therefore to study the non-radiative

loss in the singlet state, herein, we assume ii) condition, as a result, k_r^S , k_{ISC}, k_{RISC} and k_{nr}^S are approximated as follows:

$$k_r^S = \phi_p k_p + \phi_d k_d \approx \phi_F k_p \quad \text{..... (5)}$$

$$k_{RISC} \approx \frac{k_p k_d \phi}{k_r^S} \quad \text{.....(6)}$$

$$k_{ISC} \approx \frac{k_p k_d \phi_d}{k_{RISC} \phi_P} \quad \text{.....(7)}$$

$$k_{nr}^S = \frac{1-\phi}{\phi} k_r^S \quad \text{.....(8)}$$

Where, total PL quantum efficiency (Φ) = $\Phi_F + \Phi_{TADF}$.

Thus, rate constants values of TADF emitters evaluated using equations (1-4) and equations (5-8) are summarized in Table 1 of the main manuscript.

7. Device structure, characterization, and fabrication

7.1. Device structures and materials

To evaluate the device performances of TADF emitters, following OLED structures were fabricated. For the fabrication of sky blue TADF-OLEDs, mCP was chosen as blue host material and new TADF materials δ-2CbPN, α-2CbPN as dopant. Similarly, for deep blue TADF-OLEDs DBFPO and CzDCbTrz was used as host and dopants, respectively. In addition, 2CzPN, TCzTrz were used as reference emitters. Herein, 1,4,5,8,9,11-hexaazatriphenylene-hexacarbonitrile (HATCN), 1-bis((di-4-tolylamino)phenyl)cyclohexane (TAPC), 4,4,4-tris(N-carbazolyl)-triphenylamine (TCTA), and 3,5-di(9H-carbazol-9-yl)-N,N-diphenylaniline (DCDPA)[3] were used as hole transport layers. Likewise, 1,3,5-tri(m-pyrid-3-yl-phenyl) benzene (TmPyPB), diphenylphosphine oxide-4-(triphenylsilyl)phenyl (TSPO1), 2,2',2"-(1,3,5-benzinetriyl)-tris(1-phenyl-1-H-benzimidazole) (TPBi) as electron transport layers. These transport materials have appropriate triplet energy to block the triplet exciton quenching from the emissive layer. The fabricated device structures are as follows:

- **2-CzPN**, **δ-2CbPN** and **α-2CbPN** devices: ITO (50 nm) / HATCN (7 nm) / TAPC (55 nm) DCDPA (10 nm) / mCP: 20 wt% TADF emitter (20 nm) / TmPyPB (35 nm) / LiF (1.5 nm) / Al (100 nm)

- **TCzTrz** and **CzDCbTrz** devices: ITO (50 nm) / HATCN (7 nm) / TAPC (30 nm) / TCTA (20 nm) / mCP (10 nm) / DBFPO: 40 wt% TADF emitter (25 nm) / TSPO1 (5 nm) / TPBi (25 nm) / LiF (1.5 nm) / Al (100 nm)

7.2. Device fabrication and characterization

To fabricate the blue TADF OLEDs, Indium-tin-oxide (ITO, 50 nm) coated glass substrates were sequentially cleaned in ultrasonic bath with acetone and isopropyl alcohol for 10

minutes each, and rinsed with deionized water. Finally, all substrates were dried using nitrogen followed by UV-ozone treatment for 10 minutes. All organic layers and aluminum cathode were deposited on pre-cleaned ITO substrates using thermal evaporation system under vacuum pressure of ~1 x 10^{-7} Torr. The deposition rate of all organic layers was kept around 0.5 Å/s. The deposition rate of lithium fluoride (LiF) and Al cathode was maintained at 0.1 Å/s and 5 Å/s, respectively. After the deposition process, all devices were encapsulated using cover glass and UV curable resin inside the nitrogen filled glove box.

The emissive area of all the samples was 4 mm^2. Current density versus voltage versus luminance (*J-V-L*) characteristics of fabricated OLEDs were measured by using Keithley 2635A SMU and Konica Minolta CS-100A, respectively. Electroluminescent spectra and Commission Internationale de l'Eclairage (CIE) 1931 color coordinate were examined using Konica Minolta CS-2000 spectroradiometer. All measurements were performed in ambient condition.

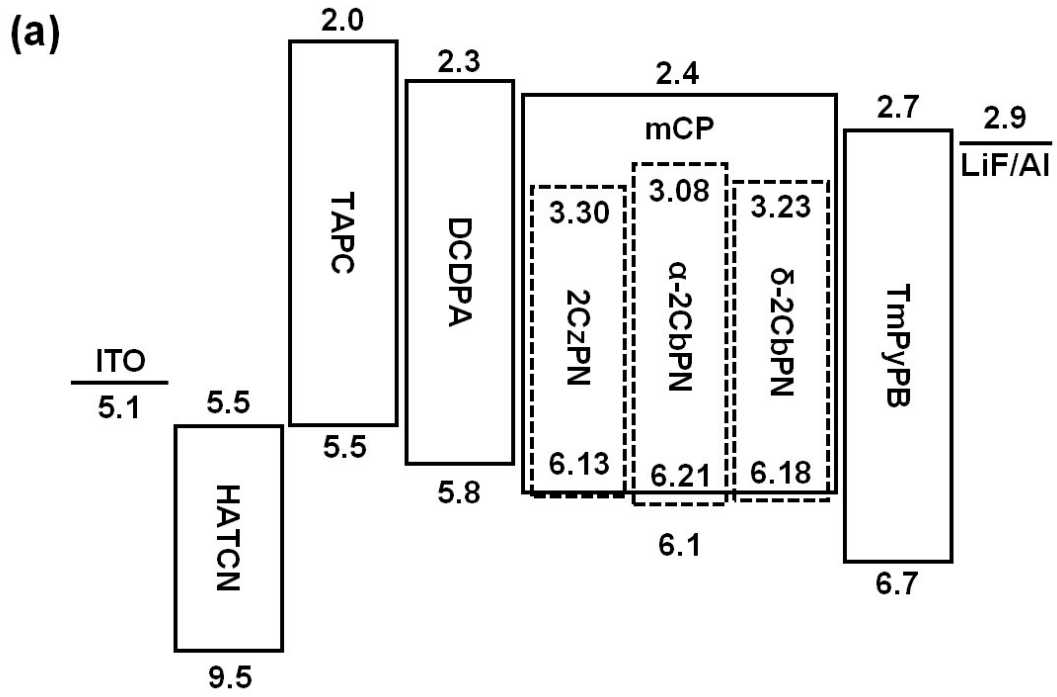

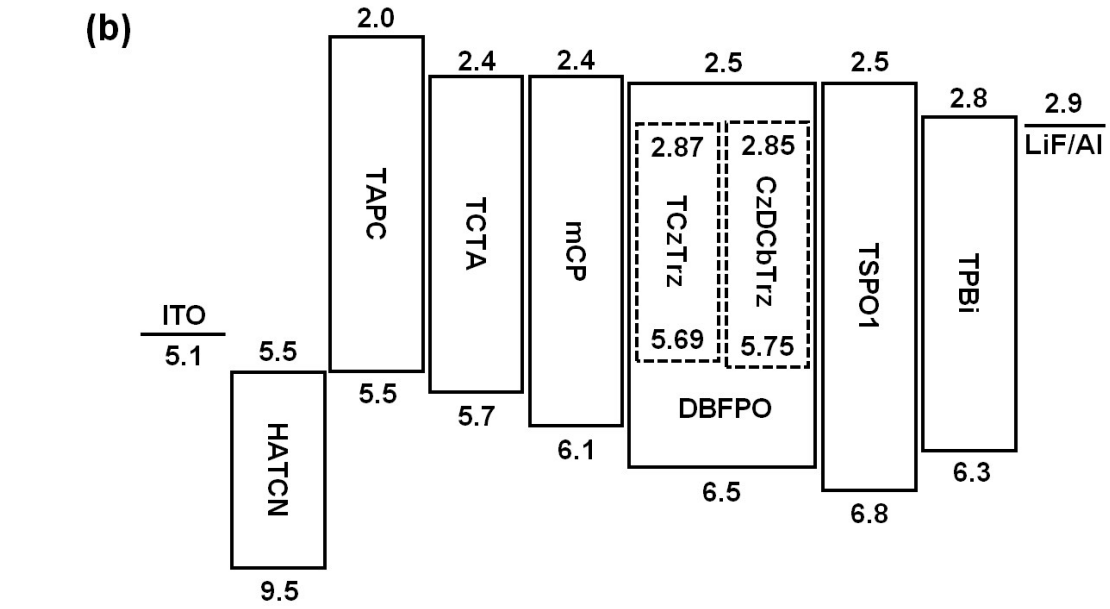

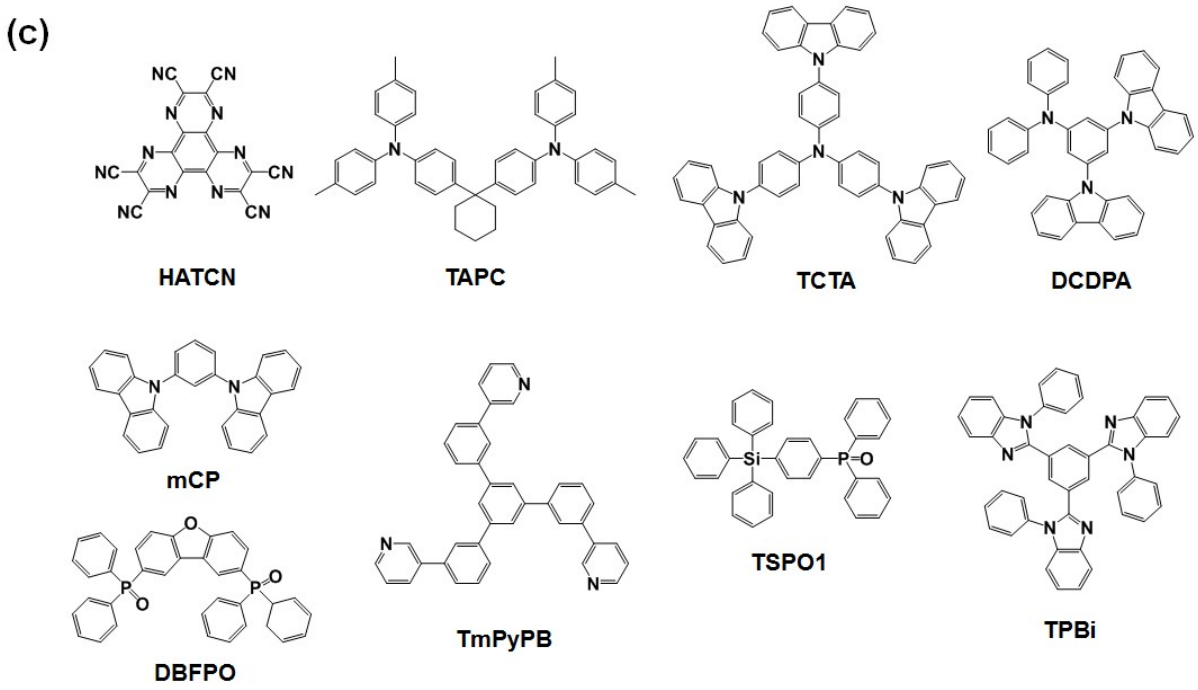

Fig. S15 Device structures of (a) **2CzPN**, **α-2CbPN** and **δ-2CbPN** (b) **TCzTrz**, **CzDCbTrz** and (c) Molecular structures of charge injection and transport materials as well as host materials used in fabricated OLEDs.

8. Device performances

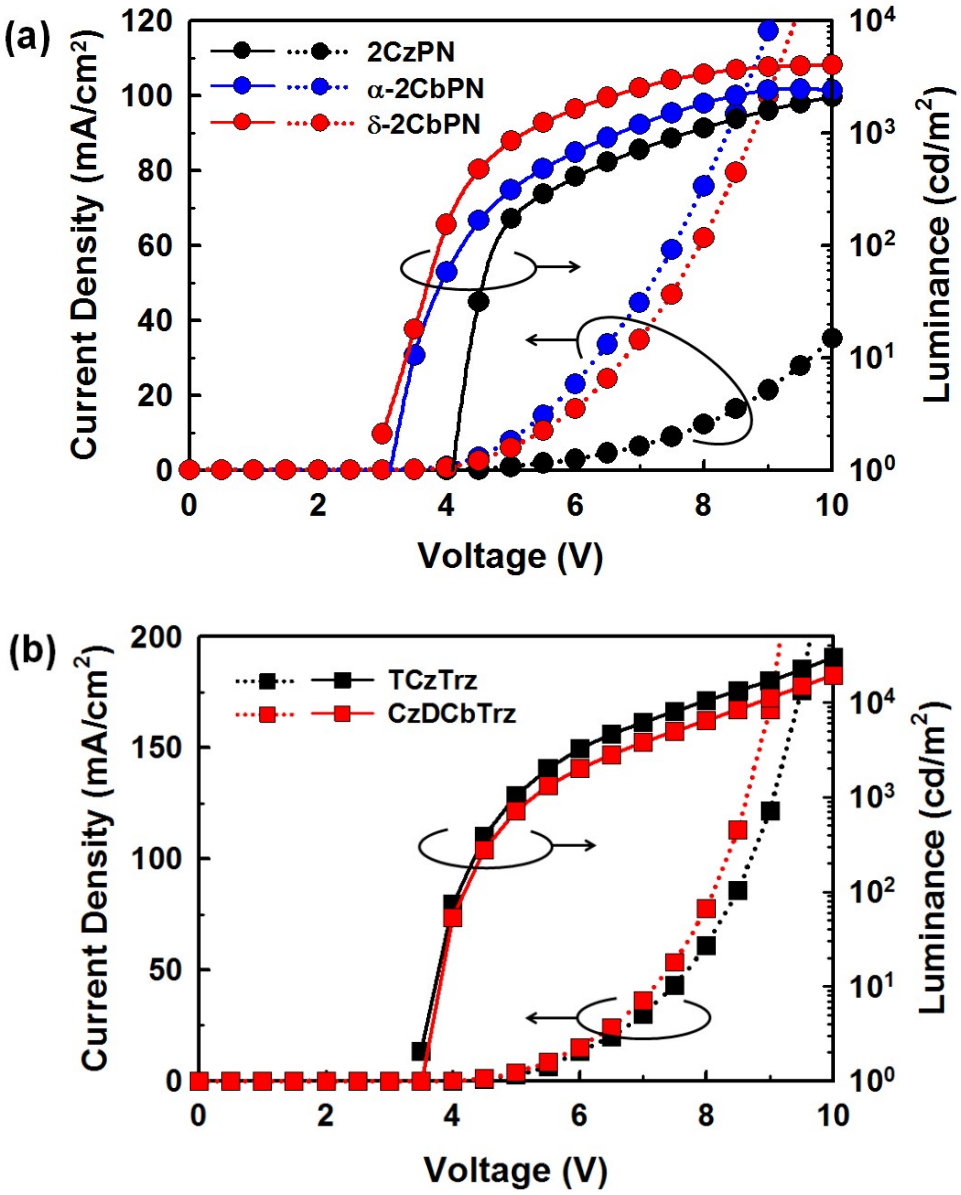

Fig. S16 *J-V-L* characteristics of blue TADF-OLEDs with (a) **2CzPN**, **α-2CbPN** and **δ-2CbPN** (b) **TCzTrz**, **CzDCbTrz** emitters.

Table S3 Comparison of fabricated blue TADF-OLEDs performances

Emitters	Operating voltage [V]	Current efficiency [cd/A]	Power efficiency [lm/W]	EQE [%]	CIE 1931 color (x, y)
	@ 1 cd/m^2 / @ 1,000 cd/m^2	Max. / @ 1,000 cd/m^2	Max. / @ 1,000 cd/m^2	Max. / @ 1,000 cd/m^2	(@ 1,000 cd/m^2)
2CzPN	4.1 / 7.8	30.1 / 10.4	27.1 / 4.1	19.2 / 6.1	(0.18, 0.36)
α-2CbPN	3.1 / 6.6	7.8 / 2.7	7.0 / 1.3	4.2 / 1.4	(0.16, 0.19)
δ-2CbPN	2.8 / 5.2	37.5 / 11.8	33.6 / 6.7	22.5 / 7.7	(0.19, 0.34)
TCzTrz	3.4 / 5.5	34.1 / 16.3	30.6 / 9.3	19.8 / 8.2	(0.17, 0.29)
CzDCbTrz	3.5 / 5.3	35.0 / 17.2	31.6 / 10.5	22.0 / 9.4	(0.16, 0.23)

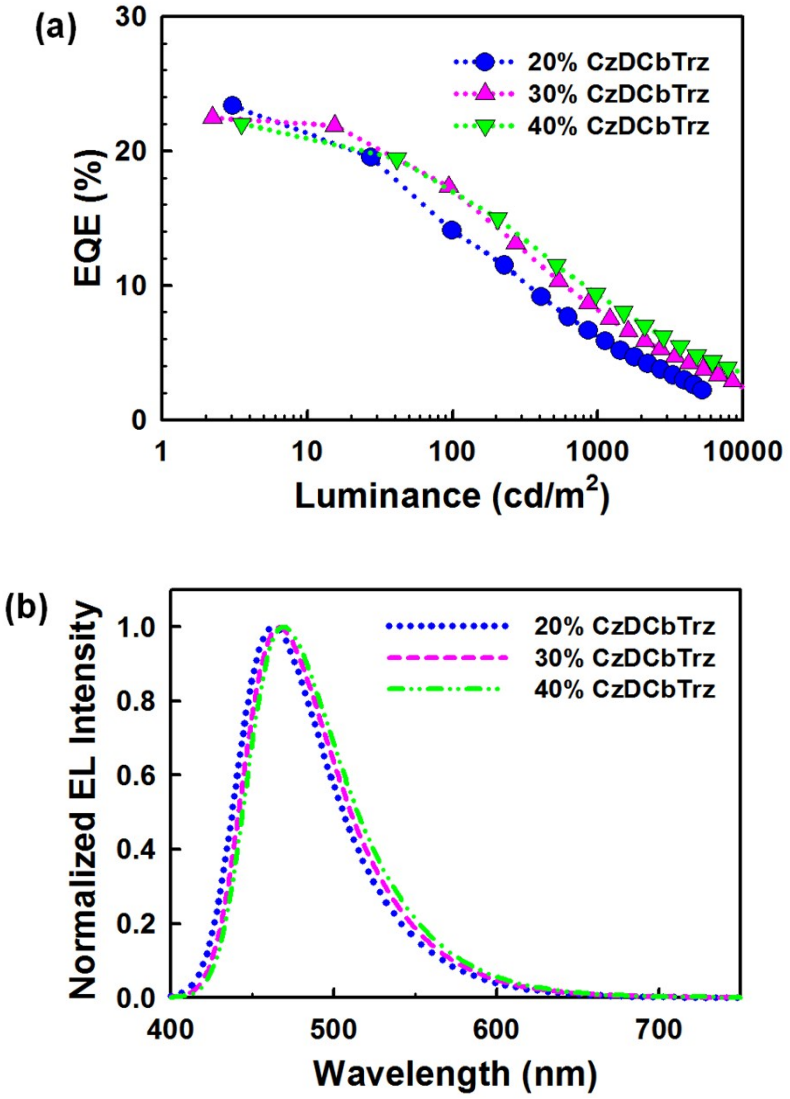

Fig. S17 (a) External quantum efficiency (EQE) versus luminance characteristics of 20, 30, and 40% **CzDCbTrz** devices (b) Electroluminescent spectra at 1,000 cd/m^2.

Table S4 Electroluminescent device performances with different doping concentration of the emitters.

Emitters	Operating voltage [V]	Current efficiency [cd/A]	Power efficiency [lm/W]	EQE [%]	CIE 1931 color (x, y) (@ 1,000 cd/m^2)
	@ 1 cd/m^2 / @ 1,000 cd/m^2	Max. / @ 1,000 cd/m^2	Max. / @ 1,000 cd/m^2	Max. / @ 1,000 cd/m^2	
40% TCzTrz	3.4 / 5.5	34.1 / 16.3	30.6 / 9.3	19.8 / 8.2	(0.17, 0.29)
20% CzDCbTrz	3.9 / 7.2	31.2 / 8.3	24.5 / 3.6	23.4 / 6.3	(0.16, 0.19)
30% CzDCbTrz	3.7 / 6.2	32.8 / 11.9	29.5 / 6.2	22.5 / 8.3	(0.16, 0.21)
40% CzDCbTrz	3.5 / 5.3	35.0 / 17.2	31.6 / 10.5	22.0 / 9.4	(0.16, 0.23)

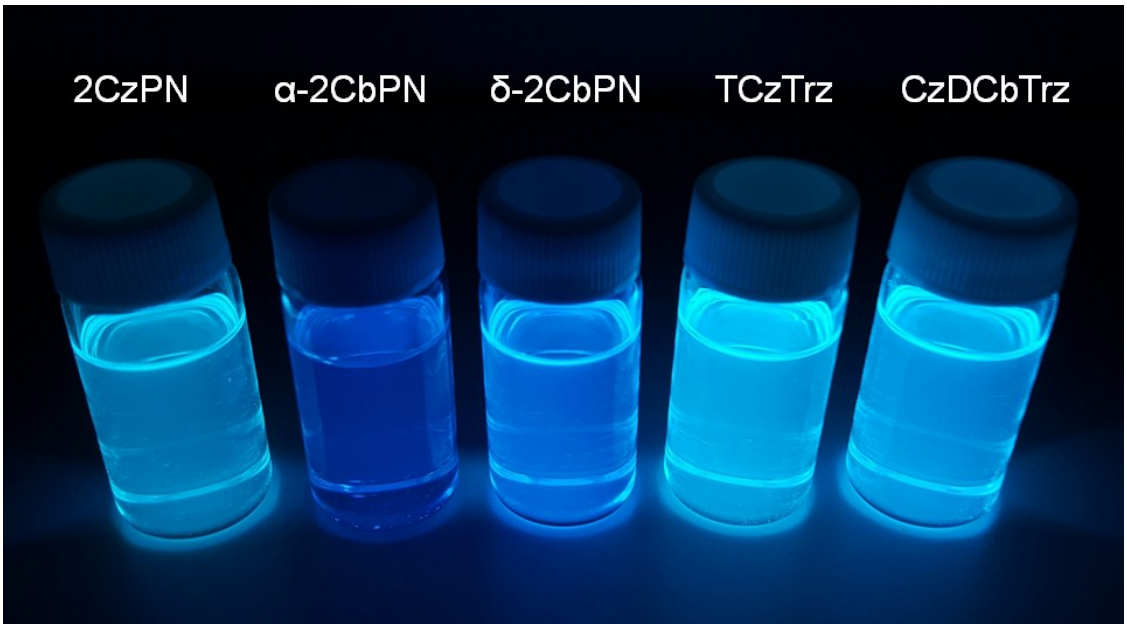

Fig. S18 Photographs of **2CzPN**, **α-2CbPN**, **δ-2CbPN**, **TCzTrz**, and **CzDCbTrz** in 10^{-5} M toluene solutions under irradiation at 365 nm wavelength.

9. Reference

1. C. C. Wu et. al, *Adv. Funct. Mater.* 2016, **26,** 7560–7571

2. K. Masui, H. Nakanotani, C. Adachi, *Org. Electron.*, 2013, **14**, 2721

3. Y. J. Cho, J. Y. Lee, *Adv. Mater.*, 2011, **23**, 4568.